Supporting Information

A Novel Bilayer Heterogeneous Poly(ionic liquid)s Electrolyte for High-Performance Flexible Supercapacitors with Ultraslow Self-Discharge

Keyi Dong,[a] Yanan Liu,[a] Zilin Chen,[a] Tian Lv,[a] Weiyang Tang,[a] Shaokui Cao,[b] Tao Chen*[a]

[a]*Shanghai Key Lab of Chemical Assessment and Sustainability, School of Chemical Science and Engineering, Tongji University, Shanghai 200092, P. R. China. E-mail: tchen@tongji.edu.cn*

[b]*School of Materials Science and Engineering, Zhengzhou University, Zhengzhou, 450001, China.*

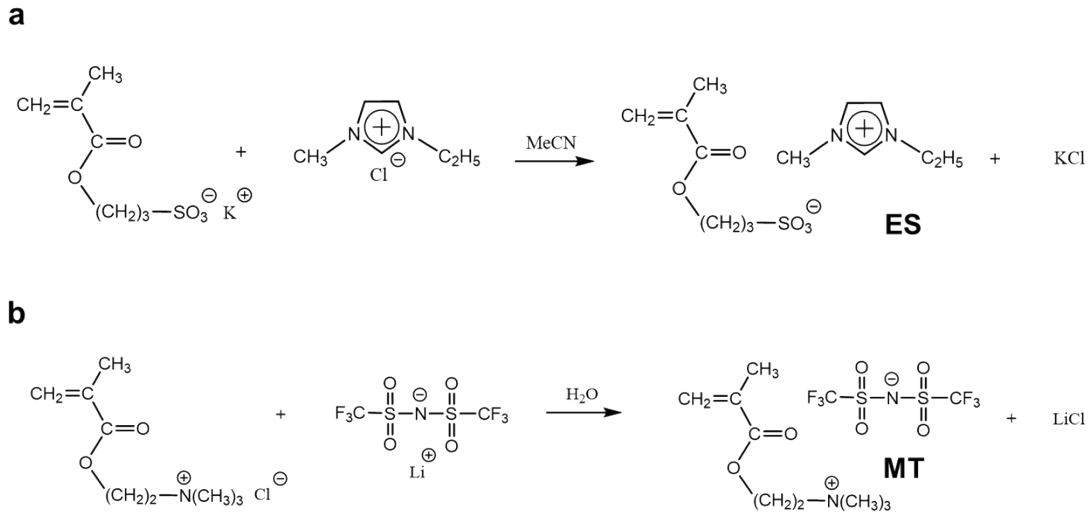

Fig. S1 Synthesis scheme of ionic liquid monomers (a) ES and (b) MT.

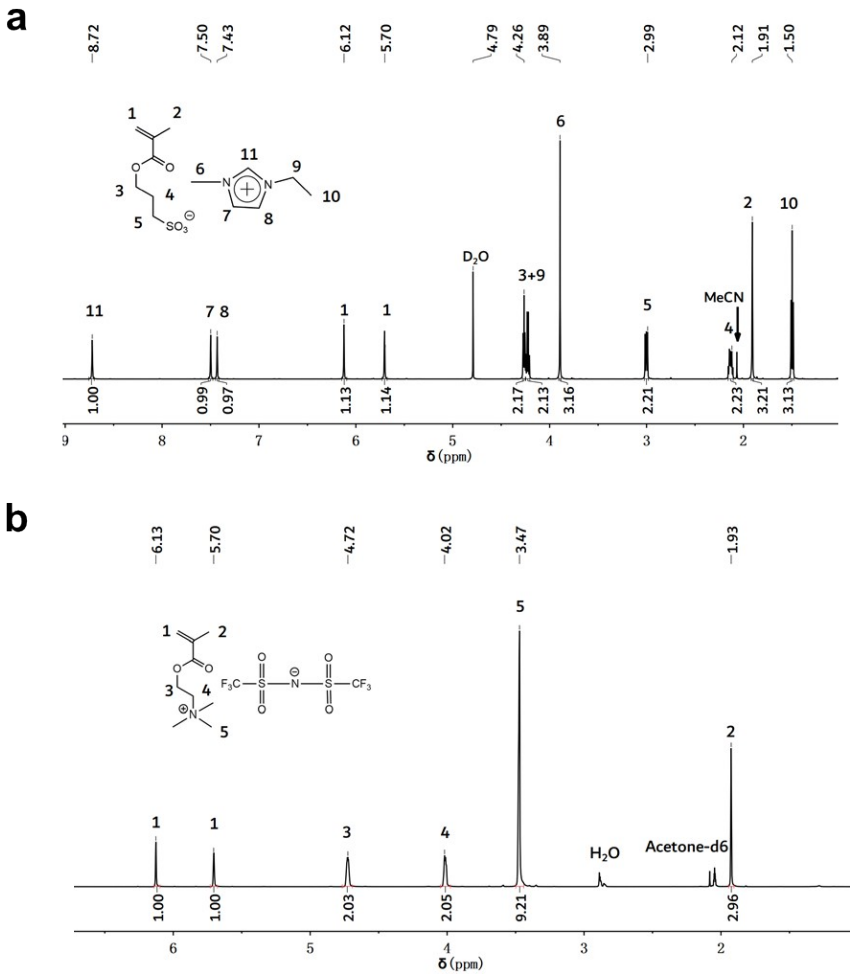

Fig. S2 ^{1}H-NMR spectrum of ionic liquid monomers (a) ES and (b) MT.

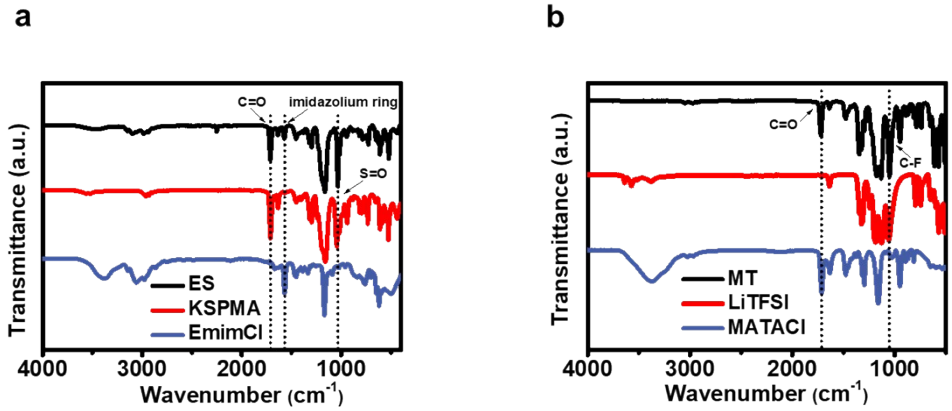

Fig. S3 FTIR spectrum of ionic liquid monomers (a) ES and (b) MT.

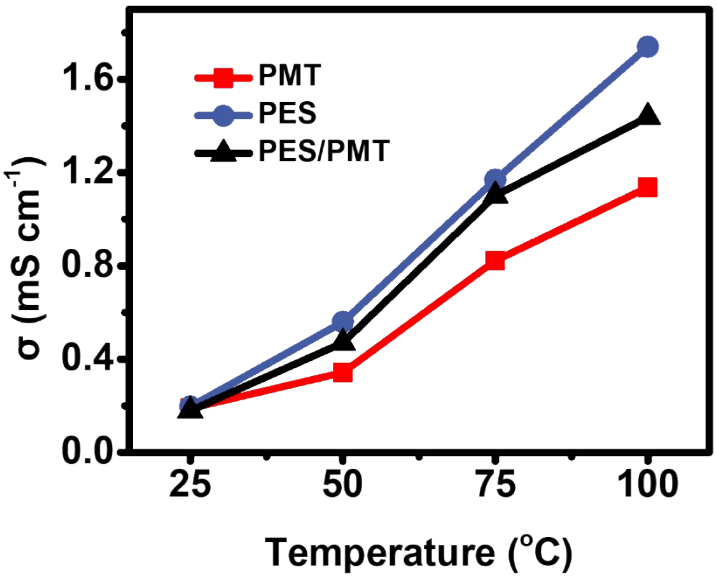

Fig. S4 Ionic conductivities of BHPE and HPE as a function of temperature.

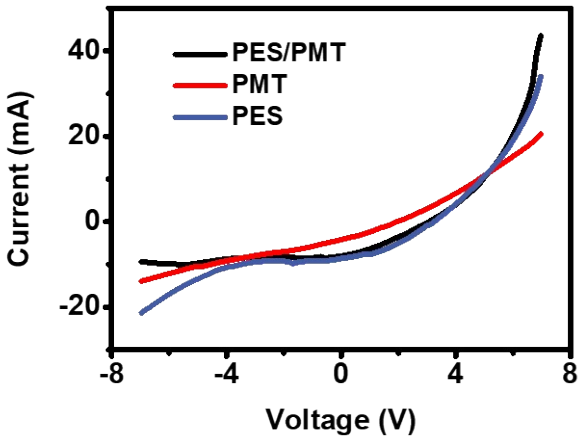

Fig. S5 I-V curves (140 mV s^{-1}) of BHPE-based and HPE-based supercapacitors by using CNTs as electrodes.

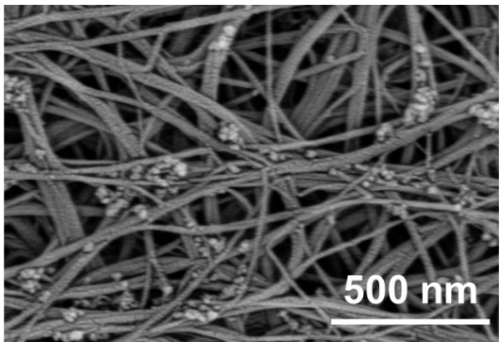

Fig. S6 Top SEM images of CNTs films.

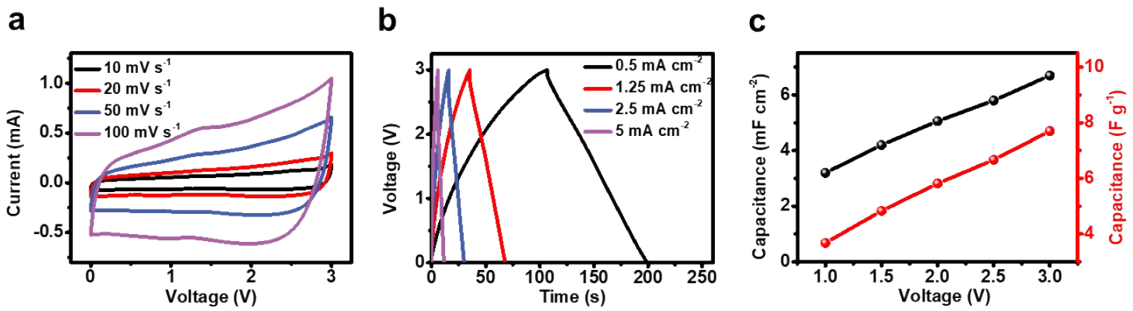

Fig. S7 Electrochemical performance of CNTs//PMT/PES//CNTs supercapacitors. (a) CV curves at different scan rates. (b) GCD curves at different current densities. (c) Areal specific capacitance and mass specific capacitance obtained at a constant current density of 0.5 mA cm^{-2} as a function of the electrochemical window.

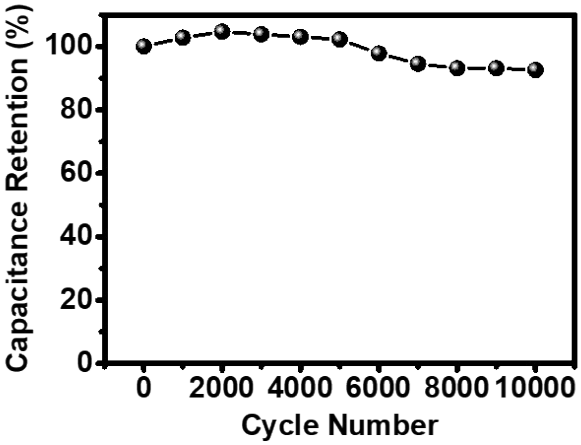

Fig. S8 Cyclic performance of CNTs//PMT/PES//CNTs supercapacitors.

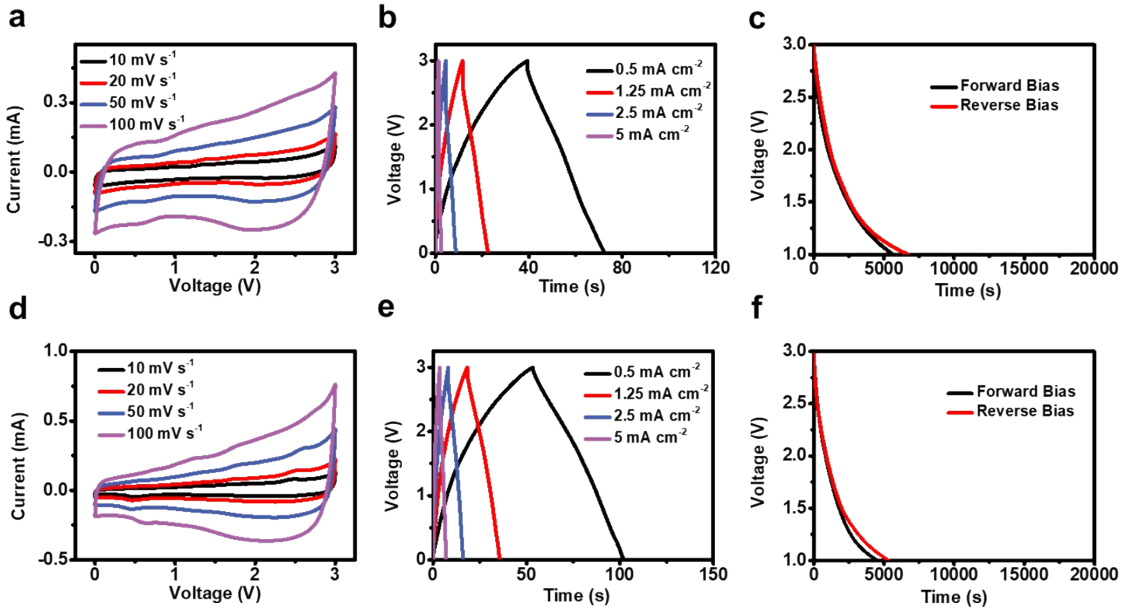

Fig. S9 CV curves at different scanning rates, GCD curves at different current densities and self-discharge curves of supercapacitors based on HPE (a-c) PMT and (d-f) PES by using CNTs as electrodes.

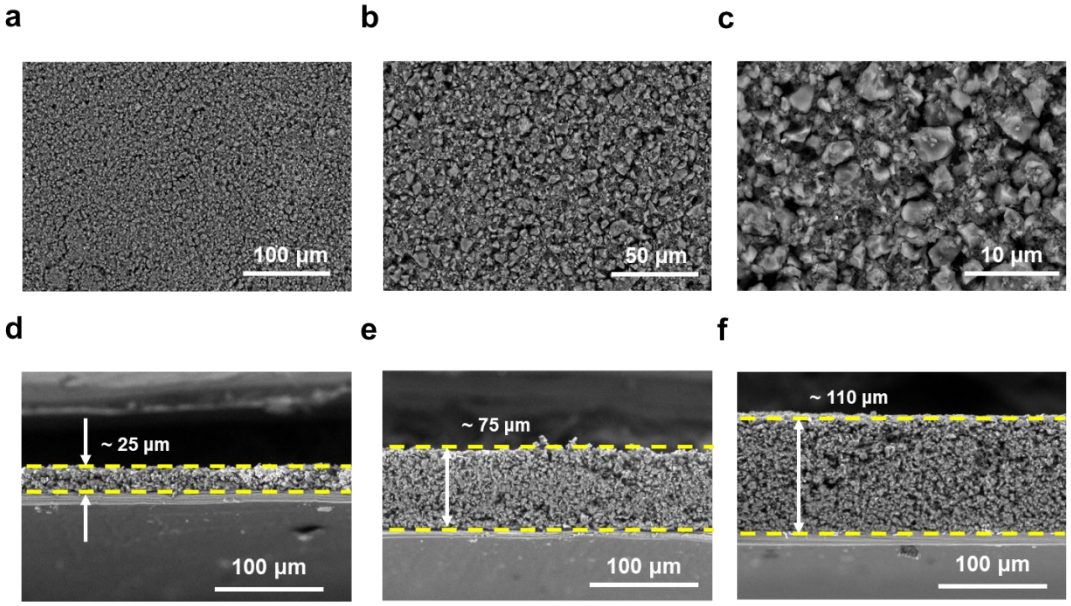

Fig. S10 (a-c) Top SEM images of AC/CNTs films. Cross-sectional SEM images of AC with the thickness of (d) 25 μm, (e) 75 μm and (f) 110 μm.

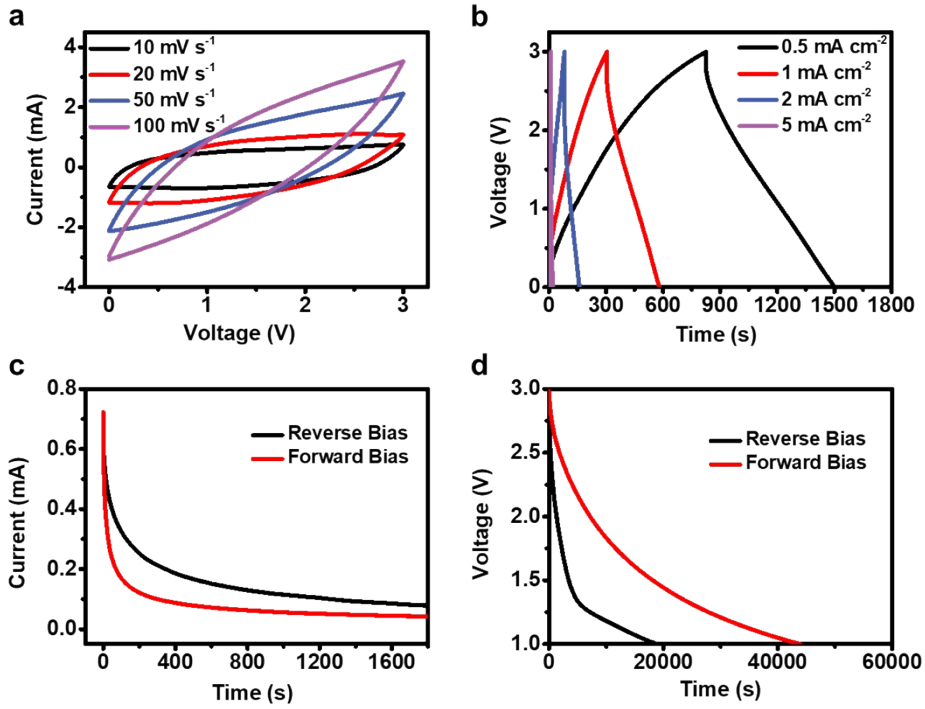

Fig. S11 Electrochemical performance of AC//PMT/PES//AC supercapacitors (The thickness of AC is 25 μm). (a) CV curves at different scanning rates. (b) GCD curves at different current densities. (c) Leakage current curves and (d) self-discharge curves under forward bias and reverse bias.

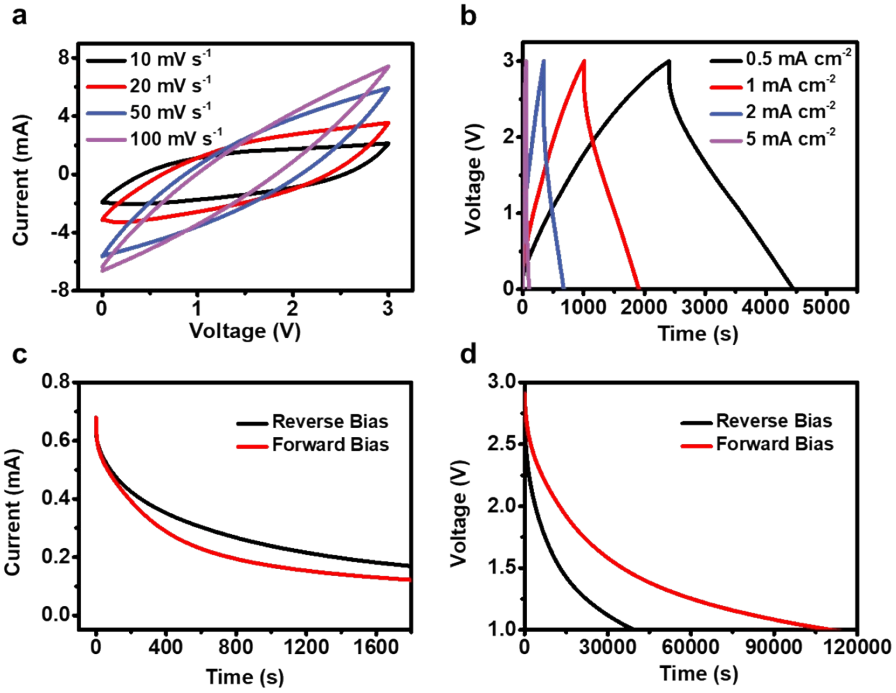

Fig. S12 Electrochemical performance of AC//PMT/PES//AC supercapacitors (The thickness of AC is 110 μm). (a) CV curves at different scanning rates. (b) GCD curves at different current densities. (c) Leakage current curves and (d) self-discharge curves under forward bias and reverse bias.

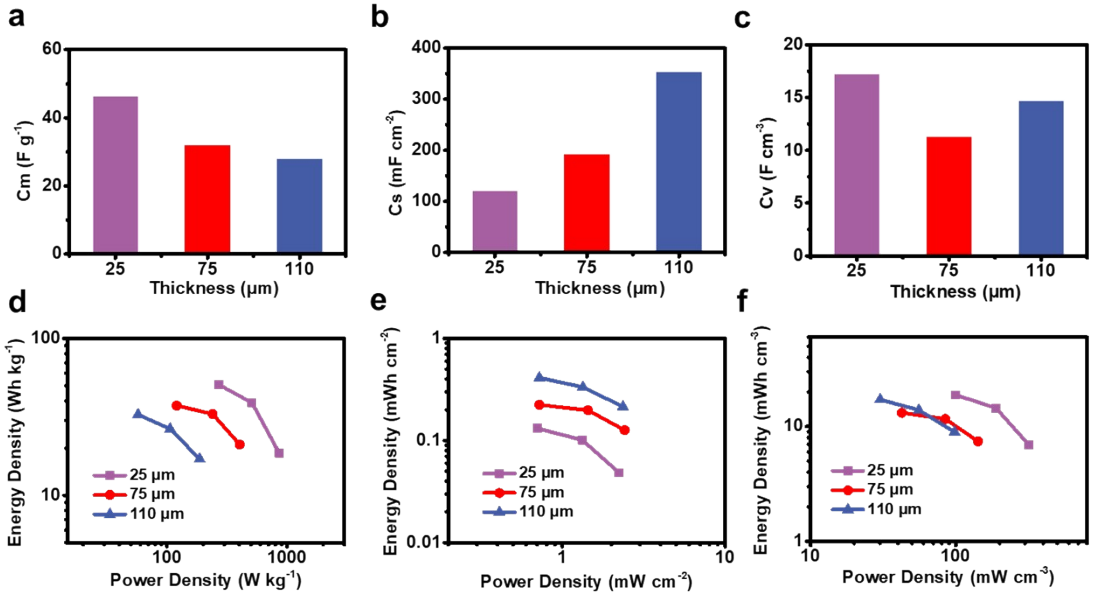

Fig. S13 (a) Volume specific capacitance, (b) areal specific capacitance and (c) mass specific capacitance of BHPE-based supercapacitors by using AC/CNTs as electrodes with different thickness of AC under a current density of 0.5 mA cm^{-2}. (d-f) Ragone plots.

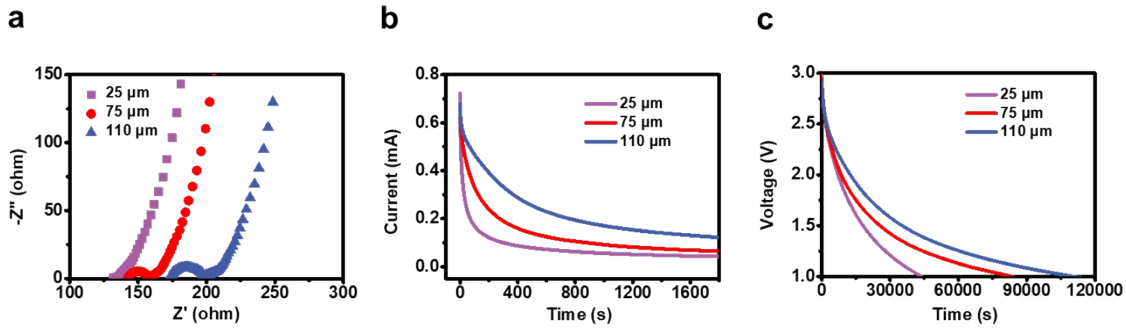

Fig. S14 Electrochemical performance of BHPE-based supercapacitors by using AC/CNTs as electrodes with different thickness of AC. (a) Nyquist plots; (b) Leakage current curves; (c) Self-discharge curves.

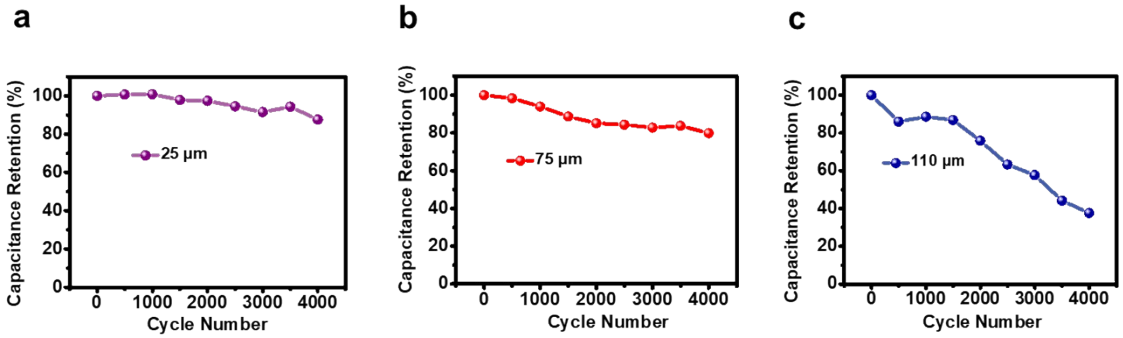

Fig. S15 Cyclic performance of AC//PMT/PES//AC supercapacitors with different thickness of AC. (a) 25 μm; (b) 75 μm; (c) 110μm.

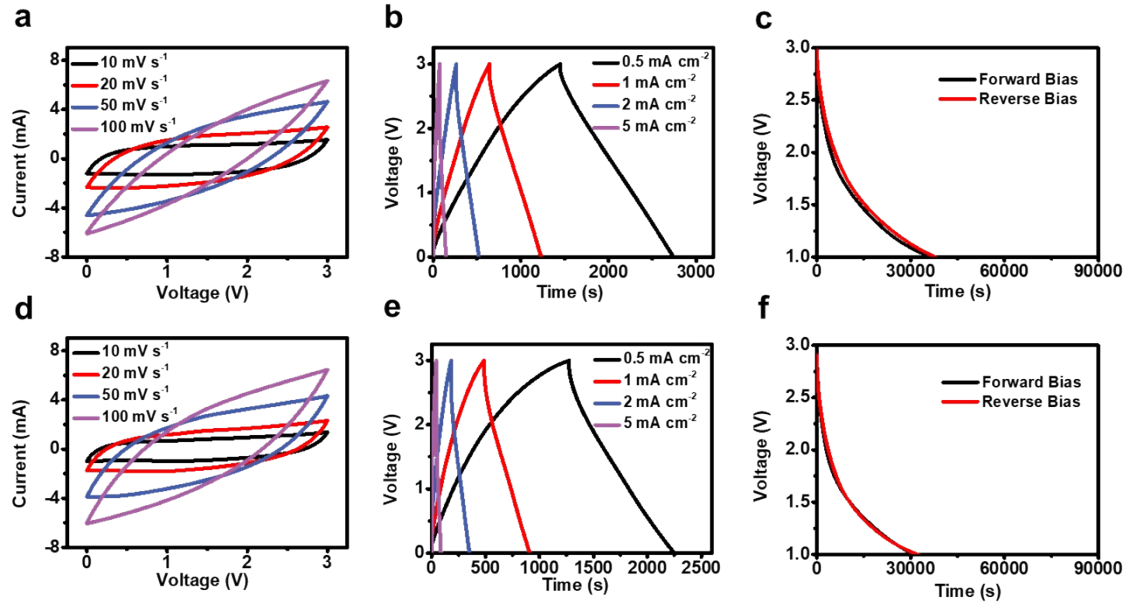

Fig. S16 CV curves at different scanning rates, GCD curves at different current densities and self-discharge curves of supercapacitors based on HPE (a-c) PMT and (d-f) PES by using AC as electrodes.

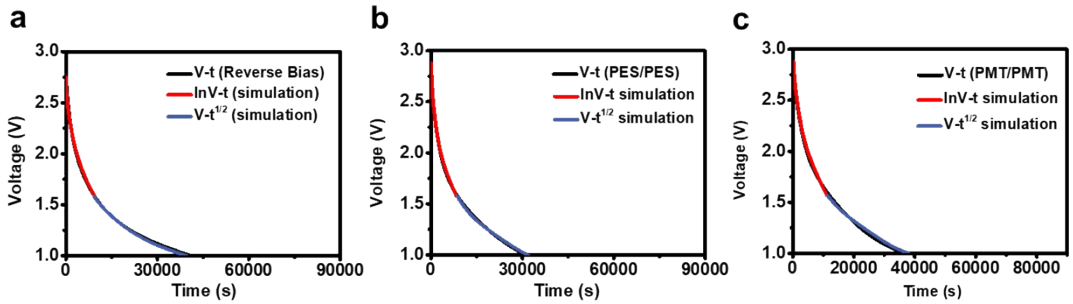

Fig. S17 Simulation by the dual-mechanism model for AC//PMT/PES//AC supercapacitors under (a) forward bias. Simulation by the dual-mechanism model for supercapacitors based on HPE (b) PES and (c) PMT by using AC/CNTs as electrodes.

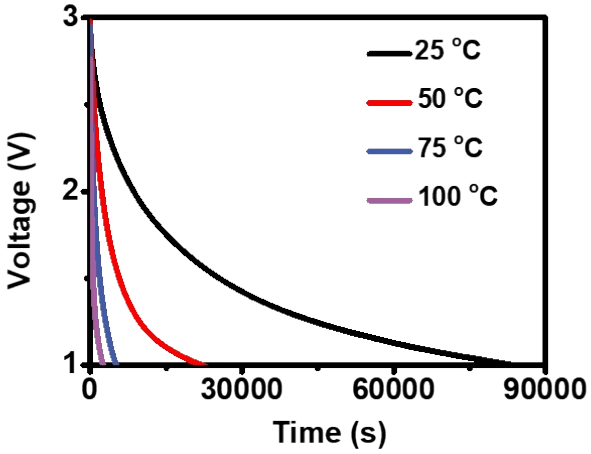

Fig. S18 Self-discharge curves of a typical BHPE-based supercapacitor under forward bias measured at different temperatures.

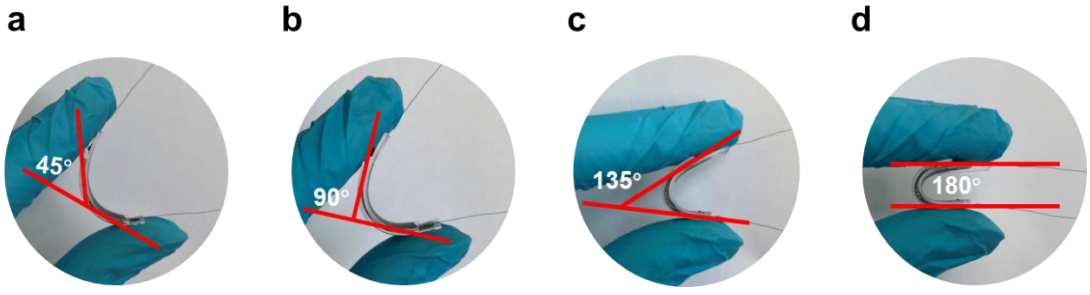

Fig. S19 Digital images of flexible supercapacitors under different bending angles.

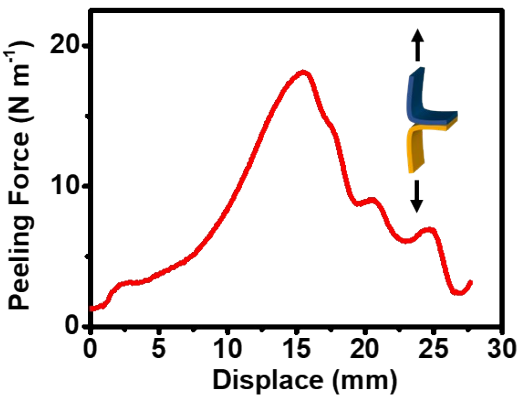

Fig. S20 The peeling force curves of BHPE.

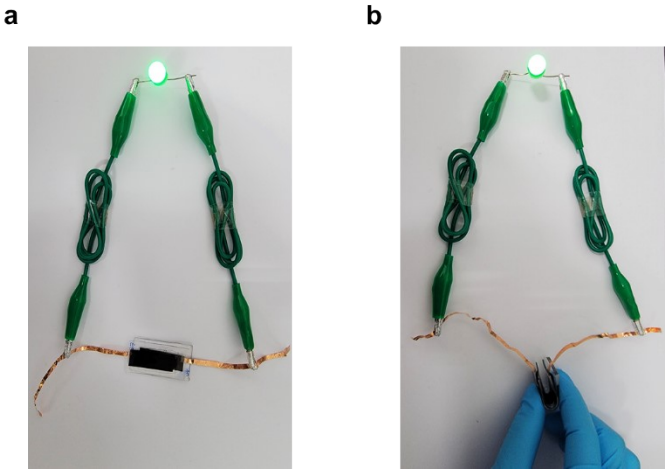

Fig. S21 Digital photographs of a single supercapacitor powering a light-emitting diode under flat state (a) and being bent to 180° (b).

Table S1 Comparison of electrochemical performance of our BHPE-based supercapacitors with those of supercapacitors with different ionic liquid as electrolytes.

Electrode	Electrolyte	Capacitance ($F\ g^{-1}$) (Single electrode)	Energy density ($Wh\ kg^{-1}$)	Power density ($W\ kg^{-1}$)	Current density ($A\ g^{-1}$)	Electro-chemical Window (V)	Cycle Life (Cycle number and capacitance retention)	Ref.
AC/CNTs	BHPE	115	33	240	0.17	3	4000, 80 %	this work
AC	PEGDA/TEGDME/LiTFSI/[Emim][TFSI]	105	23	172	0.22	2.5	10000, 85 %	[S1]
AC	PVA/Agar-[Emim][BF_4]-Li_2SO_4	28.8	4	150	0.3	1	10000, 80 %	[S2]
PEDOT/CC	PAAm/[Vmim][TFSI]	52.26	14.22	70	-	1.4	3000, 93.4%	[S3]
hierarchical porous AC	PVDF-HFP /[Emim][TFSI]	126-146	21	110	0.5	2	10000, 82 %	[S4]
AC	PVA/NaTf/[Emim][TF]	125.4	12.4	198.4	-	2	1000, 100 %	[S5]
$LiMn_2O_4$// mesoporous carbon	LiTFSI/[Emim][TFSI]	50.7	17.9	217.5	0.2	2	1000, 76 %	[S6]

Table S2 Comparison of the self-discharge time of our BHPE-based supercapacitors with those of supercapacitors with different ionic liquid as electrolytes.

Electrode	Electrolyte	Range of voltage (V)	Time of Self-discharge (h)	Ref.
AC/CNTs	BHPE	3-1	23.2	this work
α-MnO_2/N&S-rGO	PVDF-HFP [DEME][TFSI]	4.5-1.55	2	[S7]
AC	PVA/Na_2SO_4/$Pyr_{14}Br$	2-0.92	4	[S8]
AC	PVDF-HFP/[Bmim]I/CNTs	2.2-0.79	5	[S9]
AC	[Emim][FcTFSI]	2-0.7	3.3	[S10]
Porous nitrogen-doped graphene	[Bmim][PF_6]	3-0.8	10	[S11]
MnO_2@CF//FeOOH/PPy@CF	[Emim][TFSI]/FS	3.5-1	4	[S12]
PProDOT//CMK-3	PMMA/PC/[Emim][TFSI]	1.5-0.05	0.13	[S13]
PEDOP@MnO_2	PMMA/PC/[Bmim][CF_3SO_3]	0.72-0.5	0.14	[S14]
molten-salt method-derived graphene	[Emim][BF_4]	3-1.5	4.3	[S15]
AC	PVA/Li_2SO_4/BMIMI	1.5-0.64	6	[S16]

Supporting Note. The electrochemical model based on Poisson–Boltzmann equation.

Assuming a Boltzmann distribution of counterions and a uniform distribution of the fixed ions from polymer backbone, the electrostatic potential φ(z) along the z-axis of the BHPE can be described as:

$$\frac{\partial^2 \varphi(z)}{\partial z^2} = 8\pi l_b c_0 \sinh(\varphi(z)) - 4\pi l_b c_f$$

where c_0 is the local density of positive (or negative) counterions at z = 0. c_f is the density of ionic groups of PILs. $l_b=e^2/(4\pi\varepsilon T)$ is the Bjerrum length reflecting the strength of the electrostatic interaction relative to the entropic force present in the system, where ε is the dielectric constant of the medium. T is the absolute temperature and e is the elementary charge. By introducing $k_0^2=8\pi l_b c_0$ and $k_f^2=4\pi l_b c_f$, the Poisson–Boltzmann equation can be simplified as:

$$\frac{\partial^2 \varphi(z)}{\partial z^2} = k_0{}^2 \sinh(\varphi(z)) - k_f{}^2$$

The number of each of positive and negative counterions is conserved, so c_0 can be defined as:

$$\int_0^{L/2} dz c_0 \exp(\varphi(z)) = \frac{c_f L}{2}$$

where L is the length of the simulation domain.

The system is symmetric with respect to z=0, so only the right half-domain ($0 \le z \le L/2$) is taken into consideration. To solve the Poisson–Boltzmann equation, boundary conditions are applied to electrostatic potential: (i) φ(z) is zero at z=0. (ii) φ(z) is $E_{boundary}$ at z=L/2.

References

S1 D. Lee, Y. Song, Y. Song, S. J. Oh, U. H. Choi and J. Kim, *Adv. Funct. Mater.*, 2021, **32**, 2109907.

S2 H. Peng, X. Gao, K. Sun, X. Xie, G. Ma, X. Zhou and Z. Lei, *Chem. Eng. J.*, 2021, **422**, 130353.

S3 T. Mao, S. Wang, Z. Yong, X. Wang, X. Wang, H. Chen, G. Liu, D. Wang and Z. Wang, *Chem. Eng. J.*, 2021, **417**, 129269.

S4 A. A. Hor and S. A. Hashmi, *Electrochim. Acta*, 2020, **356**, 136826.

S5 J. Wang, G. Chen and S. Song, *Electrochim. Acta*, 2020, **330**, 135322.

S6 G. A. dos Santos Junior, V. D. S. Fortunato, G. G. Silva, P. F. R. Ortega and R. L. Lavall, *Electrochim. Acta*, 2019, **325**, 134900.

S7 C. Poochai, C. Sriprachuabwong, J. Sodtipinta, J. Lohitkarn, P. Pasakon, V. Primpray, N. Maeboonruan, T. Lomas, A. Wisitsoraat and A. Tuantranont, *J. Colloid Interface Sci.*, 2021, **583**, 734-745.

S8 C.-L. Geng, L.-Q. Fan, C.-Y. Wang, Y.-L. Wang, S.-J. Sun, Z.-Y. Song, N. Liu and J.-H. Wu, *New J. Chem.*, 2019, **43**, 18935-18942.

S9 L.-Q. Fan, Q.-M. Tu, C.-L. Geng, Y.-L. Wang, S.-J. Sun, Y.-F. Huang and J.-H. Wu, *Int. J. Hydrogen Energy*, 2020, **45**, 17131-17139.

S10 H. J. Xie, B. Gélinas and D. Rochefort, *Electrochem. Commun.*, 2016, **66**, 42-45.

S11 D. Liu, C. Fu, N. Zhang, Y. Li, H. Zhou and Y. Kuang, *J. Solid State Electrochem.*, 2016, **21**, 759-766.

S12 X. Gong, S. Li and P. S. Lee, *Nanoscale*, 2017, **9**, 10794-10801.

S13 S. Deshagani, A. Das, D. Nepak and M. Deepa, *ACS Appl. Polym. Mater.*, 2020, **2**, 1190-1202.

S14 A. Das, S. Deshagani, R. Kumar and M. Deepa, *ACS Appl. Mater. Interfaces*, 2018, **10**, 35932-35945.

S15 J. Wang, B. Ding, X. Hao, Y. Xu, Y. Wang, L. Shen, H. Dou and X. Zhang, *Carbon*, 2016, **102**, 255-261.

S16 Q.-M. Tu, L.-Q. Fan, F. Pan, J.-L. Huang, Y. Gu, J.-M. Lin, M.-L. Huang, Y.-F. Huang and J.-H. Wu, *Electrochim. Acta*, 2018, **268**, 562-568.